


Creating a cross-sectional, CT and MR atlas of the Pannon minipig

Ors Petnehazy^{1,2}  | Tamas Donko^{1,2} | Rosie Ellis⁷ | Adam Csoka^{1,2} |
Kalman Czeibert⁵ | Gabor Baksa⁶ | Eric Zucker⁸ | Krisztina Repa^{3,4} | Aliz Takacs¹ |
Imre Repa^{1,3} | Mariann Moizs⁴

¹Medicopus Nonprofit Ltd, Kaposvar, Hungary

²Kaposvar Campus, Szent Istvan University, Kaposvar, Hungary

³Radiation Oncology, Research and Teaching Center, Moritz Kaposi General Hospital Dr. József Baka Diagnostic, Kaposvar, Hungary

⁴Moritz Kaposi General Hospital, Kaposvar, Hungary

⁵Department of Ethology, Institute of Biology, Eötvös Loránd University, Budapest, Hungary

⁶Department of Anatomy, Histology and Embryology, Semmelweis University of Medical Sciences, Budapest, Hungary

⁷The Veterinary Referral & Emergency Centre, Godstone, England

⁸Veterinary Medicine Program, University of Alaska Fairbanks, Fairbanks, AK, USA

Correspondence

Ors Petnehazy, Medicopus Nonprofit Ltd., H-7400 Kaposvar, Guba S. str. 40, Hungary. Email: petnehazy.ors@sic.medicopus.hu

Funding information

Janos Bolyai Research scholarship of the Hungarian Academy of Sciences, Grant/Award Number: BO 921_19

Abstract

Purpose: The purpose of this study was to create a detailed cross-sectional anatomical reference atlas of the Pannon minipig by correlating good resolution CT and MR images with high quality cross-sectional anatomical images. According to the authors knowledge, no detailed anatomical atlas is available for the minipig.

Material and method: An adult female minipig was utilized for this purpose. The animal was placed in a PVC half tube, and CT generated images of 0.6 mm slice thickness and MR images of 1.41 mm slice thickness were obtained. The images covered the whole body from the most rostral portion of the snout to the tip of the tail. The CT and MR scans were aligned with frozen anatomical sections prepared with an anatomical band saw from the same animal and significant structures were identified and labelled. The terminology employed has been referenced from the *Nomina Anatomica Veterinaria 6th edition-2017*.

Findings and conclusions: The resulting atlas consists of 109 anatomical slices and the corresponding 109 CT and 109 MR scans (altogether 327 images) and the nomenclature list for each image. Although this publication contains limited images of the resulted atlas, it is a reference source for anatomy education and clinical sciences. We are of the opinion that more comprehensive and especially online available interactive atlases should be prepared using similar methodology.

KEYWORDS

3D reconstruction, 3DSlicer, cross-sectional anatomy, CT anatomy, minipig, MR anatomy

1 | INTRODUCTION

The domestic pig is one of the principal species utilized as an animal model in preclinical studies, research, education and training. Due to their physiological and anatomical similarities to the human organism, they are one of the primary species in large

animal studies of gastrointestinal diseases (Kararli. 1995; Ziegler et al., 2016), oncology (Schachtschneider et al., 2017), stem cell studies (Epstein et al., 2017), interventional radiology (Dondelinger et al., 1998), surgical training (Swindle, 1984) and overall in biomedical research (Simon & Maibach, 2000) or in neurosurgery (Sauleau et al., 2009).

This is an open access article under the terms of the Creative Commons Attribution-NonCommercial-NoDerivs License, which permits use and distribution in any medium, provided the original work is properly cited, the use is non-commercial and no modifications or adaptations are made.

© 2021 The Authors. *Anatomia, Histologia, Embryologia* published by Wiley-VCH GmbH.

The commercially available meat-type pig genotypes have excellent growth potential over a short period of time; therefore, they are not the ideal choice for long term, chronic studies where small or even no changes in body weight or organ sizes are desired (Swindle, 1984). Not only based on this but because of the simpler handling of the individuals makes the minipig a better option in diverse pig-based human preclinical studies (Vodicka et al., 2005; Bode et al., 2010).

Although the minipig plays an important and increasing role in preclinical studies, more detailed anatomical features of this genotype have not yet been fully determined. Several publications aimed to evaluate the craniofacial anatomy (Saka et al., 2002; Corte et al., 2017; Corte et al., 2019), creating MR-based brain atlases (Watanabe et al., 2001; Yun et al., 2011) which described the cytoarchitecture of the telencephalon amongst other brain areas of this genotype (Ettrup et al., 2010; Bjarkam et al., 2017).

The aforementioned studies offer a highly detailed description of a specific area of anatomical interest. However, there is no such work that details the entire anatomy of the whole animal depicted in good resolution on corresponding red, green and blue (RGB) images, CT and MR scans. Pioneering work of the Visible Human Project (Spitzer et al., 1996) utilized the cryomilling method for large volume anatomical specimens. Böttcher and Maierl (1999), made the first thin slice cross-sectional atlas of the dog. This technique and the reconstructions of the resulted slices was further improved for veterinary use by Park et al. (2014) and Chung et al. (2018). To achieve the best available dataset for a complete 3D reconstruction of any desired area of the specimen (i.e. the whole cryosectioned volume) this technique would be the best option. The major drawback of this procedure is its very high cost estimate. For an overall CT, MR and cross-sectional comparative anatomical atlas, a slicing technique employing a special band saw (Biodur Products, Heidelberg, Germany) is an appropriate alternative.

The widespread application of cross-sectional imaging tools (CT and MR) in animal-based human preclinical research and in veterinary diagnostics, calls for an atlas incorporating the entire anatomy of research animals. Such atlases were very useful tools before planning catheter studies, surgical interventions or evaluating diagnostic (CT, MR) images. To the best of the authors' knowledge, there are no detailed anatomical atlases encompassing the whole body of the minipig.

2 | MATERIALS AND METHODS

2.1 | Preparation of the animal for scanning

The protocol and ethical guidelines for this experiment was approved by the Government Office for Somogy County under the licence number of SOI/31/00190-6/2018.

An 18-month, 65 kg female 'Pannon minipig' was used to identify the main anatomical structures. The animal appeared clinically healthy at the antemortem inspection. The animal was prepared by intramuscular administration of 12 mg/kg ketamine-hydrochloride

(Ketamidol 100 mg/ml inj., Richter-Pharma AG, Wels, Austria), 1 mg/kg xylazine (Primazin 2% inj., Alfasan International B.V., Woerden, Netherland) and 0.04 mg/kg atropine (Atropinum sulphuricum-EGIS 1 mg/ml inj., EGIS, Budapest, Hungary). After sedation, a 22G intravenous catheter (B. Braun Melsungen AG, Melsungen Germany) was placed in the right lateral auricular vein. The animal was euthanized using intravenously administered T61 (Intervet International B.V. Boxmeer, Holland) to prevent any movement during the scanning processes avoiding artefacts. Immediately after euthanasia, the cadaver was placed on a PVC half tube in dorsal recumbency. An endotracheal tube (I.D.: 6.0 mm, O.D.: 8.2 mm, cuffed) was inserted into the animal's trachea during the CT examinations for inflating the lungs with a pressure of 20 cm H₂O. The tube was removed after completing the CT scans.

2.2 | CT scanning

The CT scan was performed at the Moritz Kaposi Teaching Hospital Dr. József Baka Diagnostic, Radiation Oncology, Research and Teaching Center (Kaposvár, Hungary) with a SIEMENS SOMATOM Sensation Cardiac CT (Multislice scanner, Siemens AG, Erlangen, Germany). Transverse slices were obtained from the tip of the rostrum to the end of the tail. The following parameters were used for scanning: 120 kV, 80 mAs, 0.6 mm slice thickness, 492 mm field of view (FOV) with isotropic voxels and a total number of 1916 slices. The reconstruction kernel was B30f. The series were saved in DICOM format.

2.3 | MR scanning

After we completed the CT scan, the PVC tube was transferred to the MR unit (Siemens Avanto, 1.5T, Siemens AG, Erlangen, Germany) avoiding any movements of the cadaver during transportation.

Transversal, T1-weighted Fast Imaging Low Angle Shot (FLASH) 3D gradient echo sequence was used for acquisition on 4 consecutive regions, covering the entire body. Scan parameters were as follows: TR 8.03 ms, TE 4.78 ms, flip angle: 20, matrix: 320 x 320, FOV 450 mm, slice thickness 1.41 mm (isotropic voxels), NEX 1. The images were reconstructed without gaps and saved in DICOM format.

2.4 | Preparation of the samples for photography

Immediately after scanning, the animal was deep frozen at -80°C in the same position as the scans were obtained. A plywood embedding box (dimensions: 1,500 x 500 x 500 mm) was manufactured and the frozen cadaver was placed within, where polyurethane (PU) resin (PN 013/80HM, Alvinplast, Budapest, Hungary) was poured around it. After resin polymerization, parts of the embedding box were removed, and the resulting PU block containing the cadaver was kept in the deep freezer (at -80°C) until sectioning.

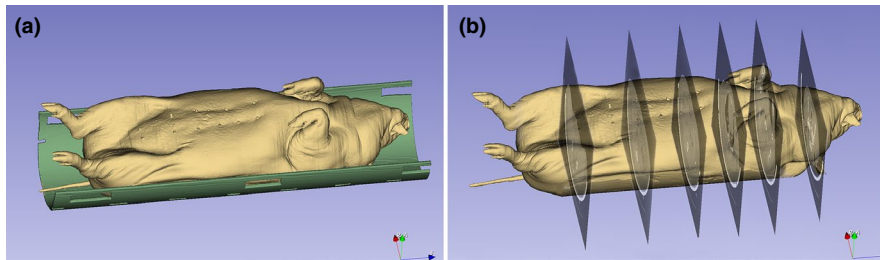


FIGURE 1 The 3D volumes reconstructed from the segmented CT-series in the 3D view of the 3D Slicer before (a) and after (b) masking out the CT table and the PVC carrying tube. The planes of the sections are represented on image B

2.5 | Slicing the cadaver

The whole block was cut with an electric band saw (Biodur Products, Heidelberg, Germany) at the Department of Anatomy, Histology and Embryology, Semmelweis University, Faculty of Medicine (Budapest, Hungary). The speed of the blade was set to 40 m/sec. A total of 144 slices were made at an average thickness of 7 mm. The slices were cleaned for photography by immersing the slices into an acetone bath and brushing off the debris from the surface.

2.6 | Photography

A Canon 5D Mark III digital camera and a Canon EF 100mm f/2.8L Macro IS USM objective was used for photographing the subsequent slices. The caudal surface of each segment was photographed for comparison with the anatomical structures of the corresponding CT and MR scans. A ColorChecker Passport Photo 2 (X-Rite, MI, USA) was captured on the corner of each slide as a reference for colour fidelity. To avoid reflections that may be caused by the comparatively wet surface of the slices, a linear polarizing filter (100 × 100 mm Square polarizer, Lee Filters, CA, USA) was mounted on the lens.

2.7 | Anatomical references

As for reference, works of Nickel et al. (Nickel et al., 2003a; Nickel et al., 2003b; Nickel et al., 2004a; Nickel et al., 2004b), Popesko (1978), Bajzik et al. (2005) and Kyllar et al. (2014) were used. The anatomical nomenclature has been referenced from the *Nomina Anatomica Veterinaria, 6th edition-2017* (<http://www.wava-amav.org/wava-documents.html>).

2.8 | Post-processing of the images and scans

The sawing resulted in 144 high quality RGB images. The proper colour balance from the camera raw data (CR2 images, Canon) based on the colour checker captured on the images and saving the images in TIFF format using UFRRAW software was made. These images were edited with Adobe Photoshop 2020 (Adobe Inc., USA) which allowed making changes in the background and slight modifications on shadow equalizing, saturation to be made if required. We removed debris (if present) on the images at photography with a clone stamp

and healing brush tool, not altering any anatomical information on the image. The anatomical structures were labelled, and the completed images were saved in .jpeg and .tiff format.

The CT and MR scans were imported to 3DSlicer (a free open source software application for medical image computing, <https://www.slicer.org>). For the CT scans, the window level (WL) was set to 260 and the window width (WW) to 3,500. During slicing the cadaver, some of the resulted slices were not perfectly at the same position where the CT and MR scans were made. We used the Reformat module in the software for both modalities (CT and MR) to correctly align the scans with the unparallelled RGB images. The resulting image was saved with the Screen capture module in PNG imaging-format and labelled with Adobe Photoshop 2020 (Adobe Inc., USA).

During identification of the anatomical structures, we opened the corresponding CT series in the Segment Editor module and created a segment for the pig's body. Using the Fast Marching effect (maximum volume: 45%, segment volume: 54.20%), we segmented the body from the outer structures (CT table, PVC carrying tube). We applied this segment as a mask to the master volume (the original CT series) and filled the outside with the Hounsfield Unit (HU) value of the air (-1024 HU). As a result, we created a volume where all the unnecessary structures outside of the minipig's body were not visible anymore (Figure 1). We opened this new Volume in the Volume rendering module (CT-Cropped-Volume-Bone preset) of the software for visualizing complete regions of the body and checking for connections and tracking of the selected structure (muscle, vessel or nerve), if needed. For this procedure, we were routinely required to crop and change the region of interest (ROI) of the selected area in the 3D view.

3 | RESULTS

The co-registering and aligning the CT and MR series with the RGB images resulted 109 triplets. Six photographs were chosen as a sample with their corresponding CT and MR images which covered the whole body and identified the clinically relevant structures. The images and photographs of the anatomical sections were positioned so that the left side (L) of the pictures is the left side of the animal and dorsal is at the top (Figures 2-7).

Our aim was to present all organs, bones and muscles within the same diagnostic image. To achieve this, we had to set the window level (WL) to 260 and the window width (WW) to 3,500 on

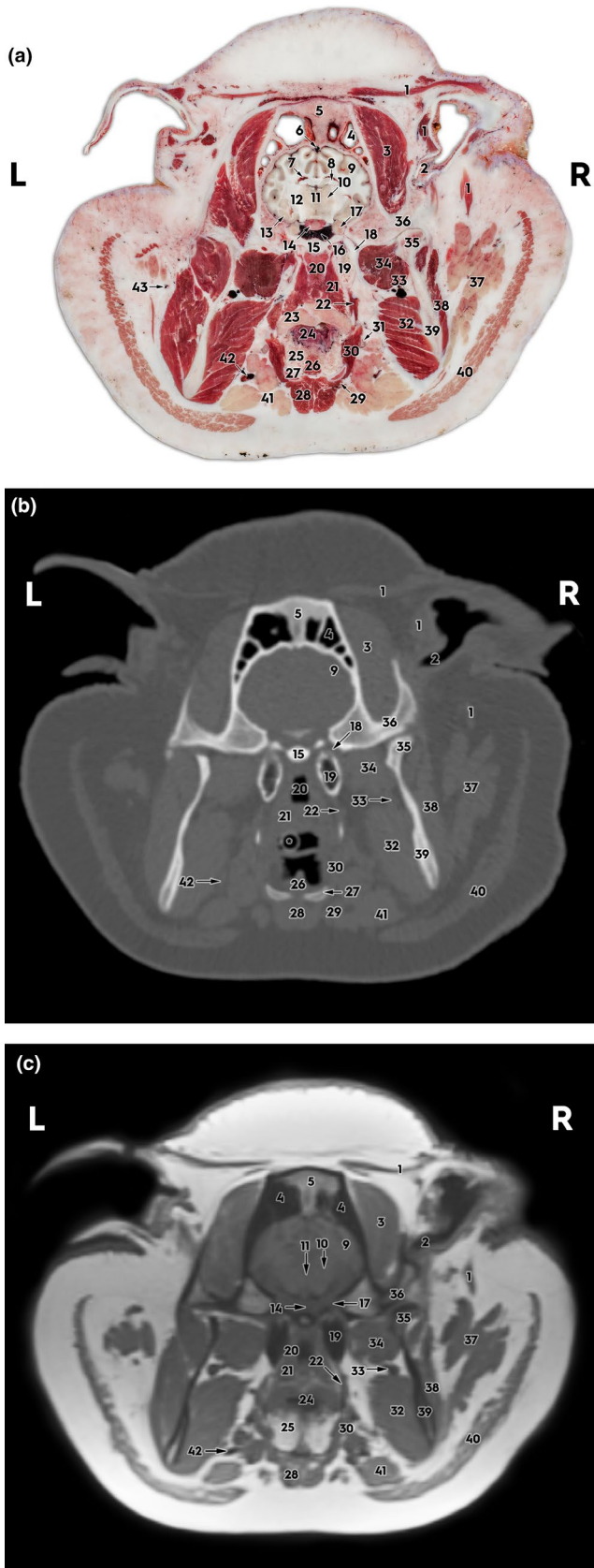


FIGURE 2 1. Mm. auriculares, 2. Meatus acusticus externus, 3. M. temporalis, 4. Sinus frontalis caudalis, 5. Os parietale, 6. Sinus sagittalis dorsalis, 7. Plexus choroideus, 8. Cornu ammonis, 9. Lobus parietalis, 10. Thalamus, 11. Adhesio interthalamica, 12. Capsula interna, 13. Lobus piriformis, 14. Hypophysis, 15. Corpus ossis basisphenoidalis, 16. Sinus cavernosus, 17. N. trigeminus, 18. N. mandibularis, 19. Bulla tympanica, 20. Nasopharynx, 21. Mm. constrictores pharynges rostrales, 22. M. levator veli palatini, 23. Tonsilla pharyngea, 24. Papillae filiformes et conicae, 25. Radix linguae, 26. M. hyoepiglotticus, 27. Basihyoideum, 28. M. sternohyoideus, 29. M. omohyoideus, 30. M. ceratohyoideus, 31. M. digastricus, 32. M. pterygoideus medialis, 33. A. v. et n. alveolaris inferior, 34. M. pterygoideus lateralis, 35. Caput mandibulae, 36. Os temporale (processus zygomaticus), 37. Gl. parotis, 38. M. masseter, 39. Ramus mandibulae, 40. Platysma, 41. Gl. submandibularis, 42. V. lingualis, 43. A. v. transversa faciei, Ramus buccalis dorsalis (N. facialis), * Endotracheal tube (on the CT scan only) a) cryosectioned (RGB) image, b) CT image, c) MR image

(the lungs, heart, large vessels and digestive apparatus). The muscle groups could be well distinguished due to the presence of intramuscular fat, which is more prevalent in the minipig than the various meat-type pig lines.

The edited and labelled image dataset and the corresponding nomenclature list for each image triplet are available online on Figshare (<https://doi.org/10.6084/m9.figshare.c.5214293>).

4 | DISCUSSION

The utilization of swine for teaching and experimental purposes in medicine and surgery has increased in the recent decades. Detailed knowledge of the desired genotype's anatomy and physiology is a prerequisite for appropriate use of pigs in teaching or as an experimental model in animal scientific studies.

Our team presented the cross-sectional anatomical atlas of the commercial pig to researchers, veterinarians, doctors and agrarians alike (Bajzik et al., 2005). This new work aimed to demonstrate the cross-sectional anatomy of the Pannon minipig.

There are many technical and biological limitations incurred through the process of creating a cross-sectional atlas. To achieve the best comparable resolution with CT data during anatomical slicing, cryosectioning with small slice thickness (below 1 mm) of the whole body would be preferable (Ackerman et al., 1995; Chung et al., 2018; Czeibert et al., 2019; Park et al., 2014; Spitzer et al., 1996). To achieve this in larger animals, such as the minipig, heavy machinery, financial resources and a technical background is required. From such a data set, three-dimensional models of any anatomical regions could be reconstructed, resulting in detailed, high quality surfaces and volumes. In our case, we cut the specimen with a band saw (Biodur Products, Heidelberg, Germany) at a slice thickness of 7 mm, resulting a good overview of the animal's entire anatomy. As the embedding block was 55 cm high, relatively large for sawing, travel time for the blade within the block was increased. Therefore, and because of the uneven nature of the

the CT scans to see both the bony and soft-tissue structures. This resulted in easy identification of the bones of the skeletal system, while allowing easy recognition of the various soft-tissue structures

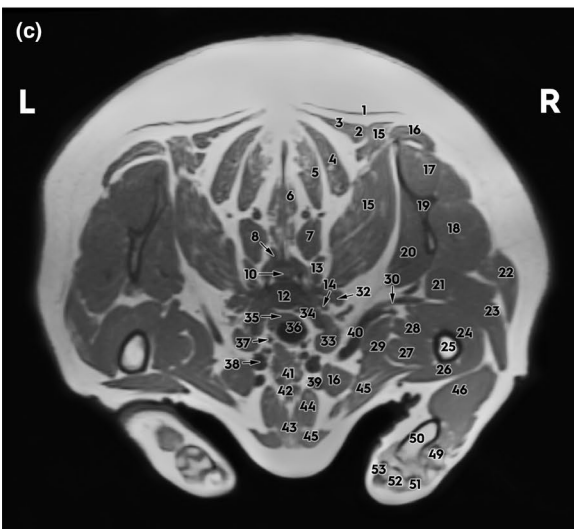
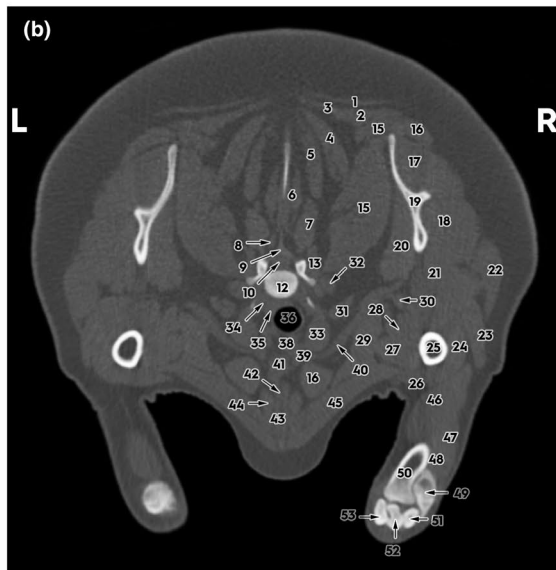
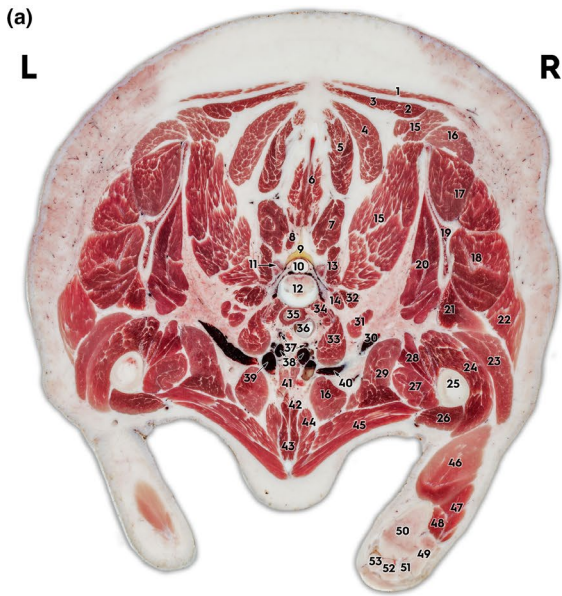


FIGURE 3 1. *M. trapezius pars cervicalis*, 2. *M. rhomboideus pars capitis*, 3. *M. rhomboideus pars cervicalis*, 4. *M. splenius*, 5. *M. semispinalis capitis (M. biventer cervicis)*, 6. *M. spinalis cervicis et thoracis*, 7. *M. complexus (M. biventer cervicis)*, 8. *Mm. multifidi*, 9. *Lig. flavum*, 10. *Medulla spinalis*, 11. *Articulatio processuum articularium C5–C6*, 12. *Vertebra C6*, 13. *M. longissimus cervicis*, 14. *Mm. intertransversarii*, 15. *M. serratus ventralis cervicis*, 16. *M. subclavius*, 17. *M. supraspinatus*, 18. *M. infraspinatus*, 19. *Scapula*, 20. *M. subscapularis*, 21. *M. triceps brachii, caput longum*, 22. *M. deltoideus*, 23. *M. triceps brachii, caput laterale*, 24. *M. brachialis*, 25. *Humerus*, 26. *M. cleidobrachialis (M. brachiocephalicus)*, 27. *M. biceps brachii*, 28. *M. teres major*, 29. *M. pectoralis profundus*, 30. *A. et v. subscapularis*, 31. *M. scalenus medius*, 32. *M. scalenus dorsalis*, 33. *M. scalenus ventralis*, 34. *M. longus colli*, 35. *Oesophagus*, 36. *Trachea*, 37. *A. carotis communis et N. vagus*, 38. *V. jugularis interna*, 39. *V. jugularis externa*, 40. *V. subclavia*, 41. *Lnn. cervicales profundi caudales*, 42. *M. sternothyroideus*, 43. *M. sternohyoideus*, 44. *M. sternomastoideus*, 45. *M. pectoralis superficialis*, 46. *M. extensor carpi radialis*, 47. *M. extensor digitorum communis*, 48. *M. abductor digiti I. longus*, 49. *Ulna*, 50. *Radius*, 51. *Os carpi ulnare*, 52. *Os carpi intermedium*, 53. *Os carpi radiale* a) cryosectioned (RGB) image, b) CT image, c) MR image

block-sharp border between the dense frozen body and the relatively soft PU foam embedding polymer around it—some of the resulting slices were uneven and not perfectly parallel.

Historically, the majority of cross-sectional atlases were made using formalin fixed cadavers (Spitzer et al., 1996; Böttcher & Maierl, 1999) or bodies with dyes injected into the vascular system (Rivero et al., 2005). Our aim was to preserve the authentic colour of the tissues to appear as fresh as possible. Thus, we euthanized the animal immediately before the scanning procedures without a perfusion of fixative through the vascular system. However, this did result in some deleterious effects. As seen on the images and scans, the minipig's body consists a massive amount of subcutaneous and intra-abdominal fat composing a good thermal-insulation layer. This heat retention sped up the bacterial post-mortem decomposing effects, particularly within the intestinal tract. This resulted in a progressive production of gas in the intestines during the prolonged whole body MR scan (1.5 hr). The followed rapid cooling of the cadaver to -80°C resulted volume changes in the intestinal tract as gases are denser at lower temperatures. Another reason for the displacement of certain structures could be the post-mortem contraction of the smooth and skeletal muscles which may have resulted in the dislocation of various parts of the digestive system compared with the CT and MR scans. This effect may be avoided by perfusing the body with low concentrations (1%–4%) of formalin. The reason we skipped cadaver perfusion was to minimize the tissue swelling and colour changes that would occur during embalming procedures (Balta et al., 2019).

There is another important factor during planning comparative atlases using CT. Since radiology and anatomy departments are separated at most universities, the anatomists have limited knowledge about the possibilities of data handling and reconstruction during and after CT imaging. There is a wide range of commercial (Amira–Thermo Fisher Scientific, Osirix–Pixmeo, Mimics–Materialize) or

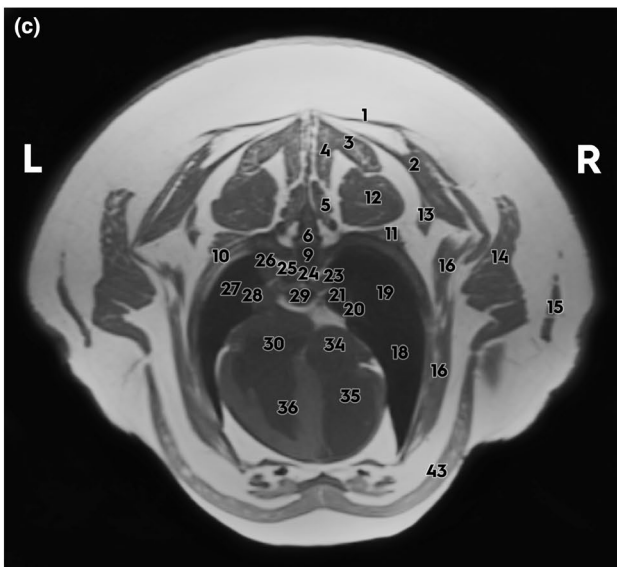
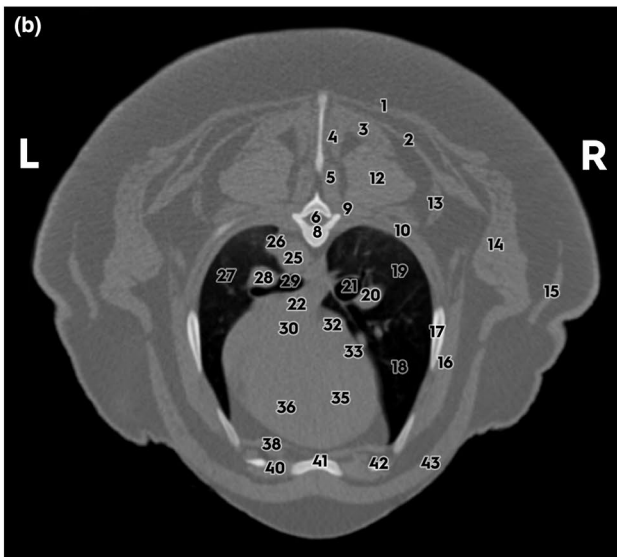
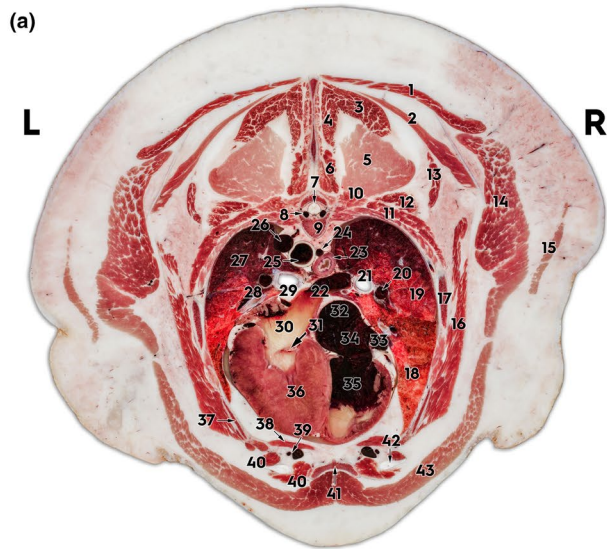


FIGURE 4 1. M. trapezius pars thoracis, 2. M. rhomboideus thoracis, 3. M. spinalis cervicis, 4. M. spinalis thoracis, 5. M. longissimus thoracis, 6. Mm. multifidi et rotatores, 7. Medulla spinalis, 8. Plexus vertebralis, 9. Vertebra Th5, 10. Mm. levatores costarum, 11. Mm. intercostales, 12. M. iliocostalis thoracis, 13. M. serratus dorsalis pars cranialis, 14. M. latissimus dorsi, 15. M. cutaneus trunci, 16. M. serratus ventralis thoracis, 17. Costa V., 18. Lobus cranialis (pulmo dexter), 19. Lobus medius (pulmo dexter), 20. V. pulmonalis lobi medii dextri, 21. Bronchus principalis dexter, 22. V. pulmonalis dexter, 23. Oesophagus, 24. A. et v. bronchooesophagea, 25. Aorta descendens, 26. V. azygos sinistra, 27. Lobus cranialis (pulmo sinister), 28. V. pulmonalis lobi cranialis sinistri, 29. Bronchus principalis sinister, 30. Atrium sinistrum, 31. Cuspis septalis (valva bicuspidalis), 32. V. cava caudalis, 33. Atrium dextrum, 34. Sinus coronarius, 35. Ventriculus dexter cordis, 36. Ventriculus sinister cordis, 37. Costa IV., 38. M. transversus thoracis, 39. A. et v. thoracica interna sinistra, 40. Mm. intercartilaginei, 41. Sternum, 42. Cartilago costae IV., 43. M. pectoralis profundus a) cryosectioned (RGB) image, b) CT image, c) MR image

freely (3D Slicer, VTK, ImageJ and more) available software offering numerous post-processing possibilities such as segmentation, a variety of registrations, image fusion, 3D modelling, etc. There is, however, an important limitation factor: the user can only import a dataset into the post-processing software which has already been reconstructed from the raw data set with a special kernel setting defined by the operator at the imaging site. If the raw data has been reconstructed with an inadequate kernel setting (i.e. sharp bone kernel for soft-tissue reconstructions), the images could contain too much noise for several post-processing options. This can be avoided if the original raw data set of the entire CT procedure is saved allowing later modification if it is reloaded to the same operational software of the vendor (Siemens in this case) (Seeram, 2013; Bertolini, 2017).

During the post-processing of the images, anatomical information was not altered under any circumstance; however, the image clarity and contrast was modified resulting in improved image quality and detail recognition. As previously mentioned, some dislocation of the inner organs occurred during freezing and as a result of post-mortem changes. Since the CT and MR images were made with isotropic voxels, we could use a reformatting option within the post-processing software (3D Slicer) to tilt the reconstructional plane to fit with the RGB image.

With CT images, it is always an inordinate challenge to select the optimal WW and WL setting for an atlas that incorporates the whole body. When interpreting CT images, radiologists optimize these window adjustments for tissues relevant to their task, and these alterations are crucial for the effective detection of some pathologies (Xue et al., 2012; Noda et al., 2018). Optimizing the presentation of any given region calls for a developed online atlas through where alterations could be made according to the viewer's needs. A majority of the online atlases currently available lack this option and contain images with predefined WW and WL settings

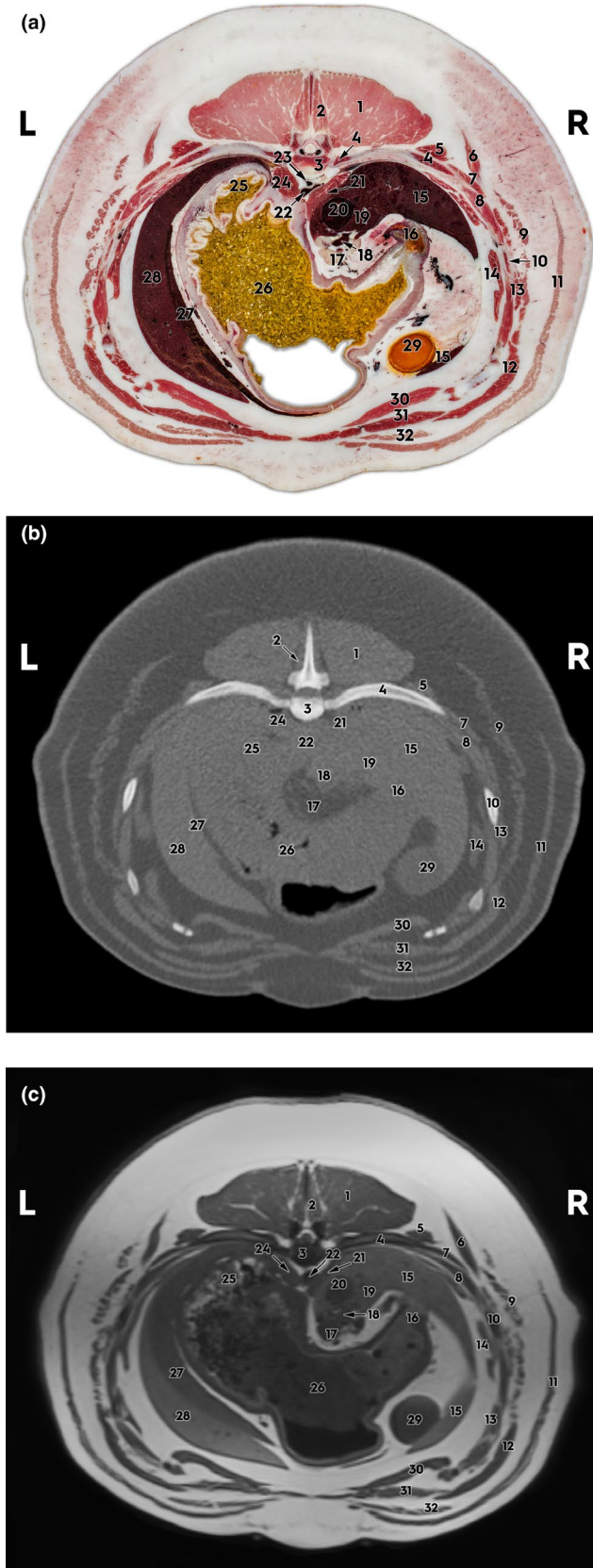


FIGURE 5 1. *M. longissimus thoracis*, 2. *Mm. multifidi et rotatores*, 3. *Vertebra Th11*, 4. *Costa XI*, 5. *M. iliocostalis thoracis*, 6. *M. serratus dorsalis pars caudalis*, 7. *Mm. intercostales externi*, 8. *Mm. intercostales interni*, 9. *M. latissimus dorsi*, 10. *Costa X*, 11. *M. cutaneus trunci*, 12. *M. obliquus externus abdominis*, 13. *M. obliquus internus abdominis*, 14. *M. phrenicus (corona muscularis)*, 15. *Lobus hepatis dexter lateralis*, 16. *Pars pylorica gastris*, 17. *Pancreas*, 18. *V. portae*, 19. *Lobus quadratus hepatis*, 20. *V. cava caudalis*, 21. *Crus dextrum (diaphragma)*, 22. *Aorta descendens*, 23. *V. azygos sinistra*, 24. *Crus sinistrum (diaphragma)*, 25. *Diverticulum ventriculi*, 26. *Fundus ventriculi*, 27. *Lien*, 28. *Lobus hepatis sinister lateralis*, 29. *Vesica fellea*, 30. *M. transversus abdominis*, 31. *M. rectus abdominis*, 32. *M. pectoralis profundus a) cryosectioned (RGB) image, b) CT image, c) MR image*

Without this interactive possibility, an atlas containing CT and MR images (like ours) will always miss the option to adjust the WW and WL settings to the optimum of the tissue examined and/or the reader's needs.

The physical limitations of MR image acquisition, such as the magnetic fields inhomogeneity outbound of the isocentre, makes imaging of larger objects, such as a pig's trunk, challenging. This may be avoided by using a higher field strength MR scanner or utilizing prolonged image acquisition times (Westbrook & Talbot, 2018).

Even with T1-weighted images the signal intensity of fat is very high. Since the minipig has an extremely high body fat content, both subcutaneous and intra-abdominal, it proved a challenge to determine the most appropriate setting during image acquisition. In images obtained of the trunk, especially closer to the skin, areas of very high signal intensity could be observed. Fat-suppression sequences are available in MR imaging, like fat saturation, inversion recovery, opposed phase imaging (Delfaut et al., 1999; Bley et al., 2010; Westbrook & Talbot, 2018), and there are special requirements at high field-strength equipment (Del Grande et al., 2014). All these sequences have advantages and disadvantages for constructing clear anatomical images, especially at a larger FOV where the inhomogeneity of the magnetic field plays a significant role in image quality.

5 | CONCLUDING REMARKS

As the minipig becomes increasingly utilized in education and medical research; particularly in human preclinical studies, so there is a growing need for comprehensive anatomical knowledge of this species. The aim of this atlas is to concisely demonstrate the anatomy of a healthy female minipig in three visual modalities. Advanced imaging techniques can, when coupled with cross-sectional anatomical preparations, clearly illustrate important topographical landmarks and their relationships to adjacent structures. Once the normal anatomy is understood and plainly depicted, gross pathological changes occurring in animal models of medical research may be better interpreted. Furthermore, with an ever-growing application of advanced imaging techniques in veterinary science and education, the ability

(www.castlemountain.dk; www.imaios.com). Few atlases offer this option (www.sectional-anatomy.org) and, to the authors' knowledge, there are no veterinary atlases online with this possibility.

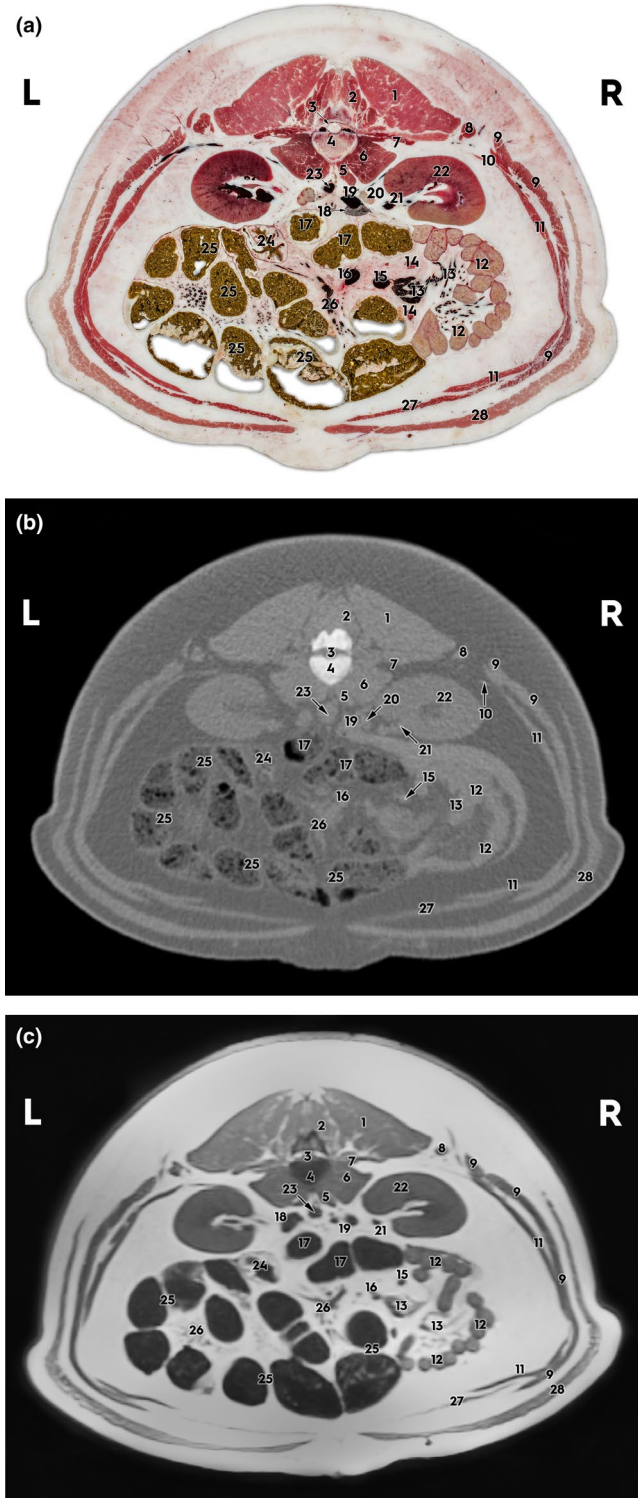


FIGURE 6 1. M. longissimus lumborum, 2. Mm. multifidi et rotatores, 3. Medulla spinalis, 4. Vertebra L2, 5. M. psoas minor, 6. M. psoas major, 7. M. quadratus lumborum, 8. M. iliocostalis lumborum, 9. M. obliquus externus abdominis, 10. M. obliquus internus abdominis, 11. M. transversus abdominis, 12. Jejunum, 13. Aa. et vv. jejunales, 14. Lnn. jejunales, 15. V. mesenterica cranialis, 16. V. ileocolica, 17. Colon descendens, 18. Duodenum transversum, 19. V. cava caudalis, 20. Glandula suprarenalis, 21. A. renalis dextra, 22. Ren dexter, 23. Aorta descendens, 24. Colon ascendens, 25. Colon (ansa spiralis coli), 26. Aa. et vv. colicae, 27. M. rectus abdominis, 28. M. cutaneus trunci a) cryosectioned (RGB) image, b) CT image, c) MR image

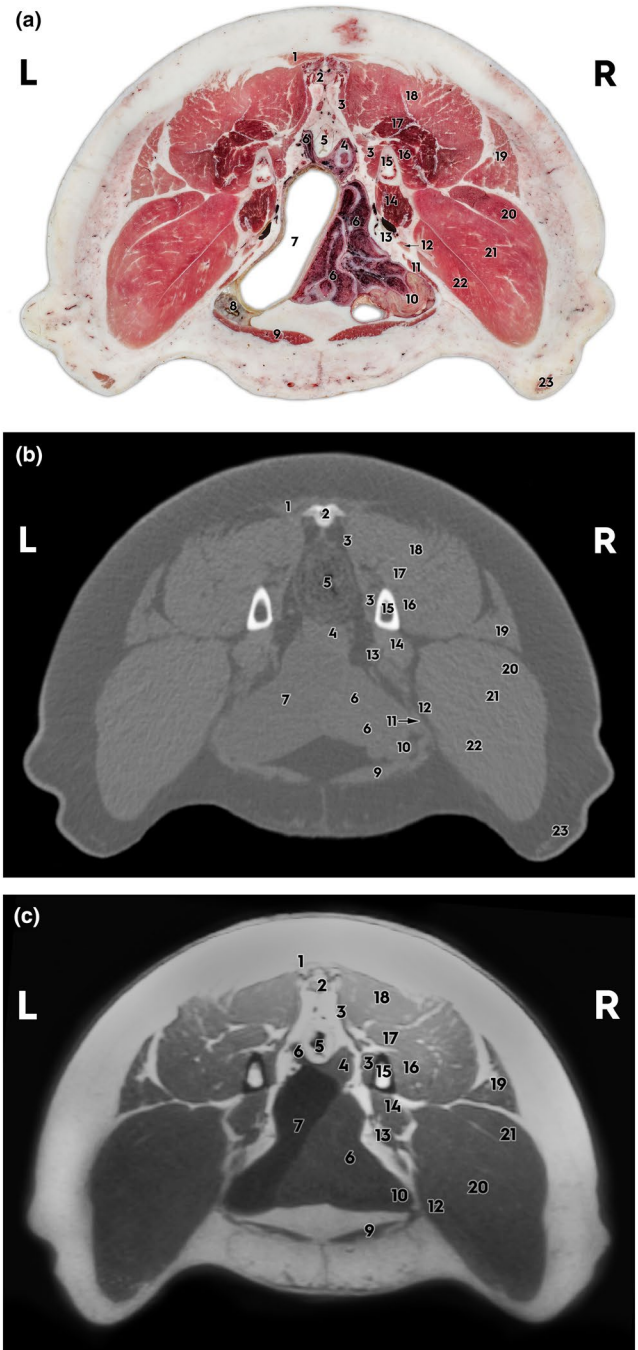


FIGURE 7 1. M. biceps femoris, 2. Vertebra coccygea, 3. M. levator ani (M. iliocaudalis), 4. Cornua uteri, 5. Rectum, 6. Cornua uteri, 7. Vesica urinaria, 8. Colon (ansa spiralis coli), 9. M. rectus abdominis, 10. Jejunum, 11. M. obliquus internus abdominis, 12. M. sartorius, 13. A. et v. iliaca externa et N. femoralis, 14. M. iliopsoas, 15. Corpus ossis ilii, 16. M. gluteus profundus, 17. M. piriformis, 18. M. gluteus medius, 19. M. tensor fasciae latae, 20. M. vastus lateralis (M. quadriceps femoris), 21. M. rectus femoris (M. quadriceps femoris), 22. M. vastus medialis (M. quadriceps femoris), 23. M. cutaneus trunci a) cryosectioned (RGB) image, b) CT image, c) MR image

to correlate structures observed in anatomical dissections or post-mortem examinations with CT and MR generated images will serve as an important clinical tool.

ACKNOWLEDGEMENT

This project was supported by the János Bolyai Research Scholarship (No. Bo/921/19) of the Hungarian Academy of Sciences.

CONFLICT OF INTEREST

The authors declare that they have no conflict of interest.

DATA AVAILABILITY STATEMENT

The dataset supporting the conclusions of this article is included in the article.

ORCID

Ors Petnehazy  <https://orcid.org/0000-0001-9698-5753>

REFERENCES

- Ackerman, M. J., Spitzer, V. M., Scherzinger, A. L., & Whitlock, D. G. (1995). The Visible Human data set: An image resource for anatomical visualization. *Medinfo*, 8(Pt 2), 1195–1198.
- Bottcher, P., & Maierl, J. (1999). Macroscopic cryosectioning: A simple new method for producing digital, three-dimensional databases in veterinary anatomy. *Anatomia, Histologia, Embryologia*, 28(2), 97–102. <https://doi.org/10.1046/j.1439-0264.1999.00171.x>
- Bajzik, G., Bogner, P., Garamvölgyi, R., Hevesi, Á., Horn, P., Lőrincz, B., Petneházy, Ö., Petrás, Z. S., Romvári, Z. R., Szladovits, Z. S., & Szladovits, Z. S., Vajda, Z. S. (2005). *Cross-sectional CT and MR anatomy atlas of the domestic pig*. Retrieved from <http://link.oszk.hu/libriurl.php?LN=hu&DB=any&SRY=an&SRE=000002583036>
- Balta, J. Y., Twomey, M., Moloney, F., Duggan, O., Murphy, K. P., O'Connor, O. J., Cronin, M., Cryan, J. F., Maher, M. M., & O'Mahony, S. M. (2019). A comparison of embalming fluids on the structures and properties of tissue in human cadavers. *Anatomia, Histologia, Embryologia*, 48(1), 64–73. <https://doi.org/10.1111/ah.12412>
- Bertolini, G. (2017). *Body MDCT in Small Animals: Basic Principles, Technology, and Clinical Applications*. <https://doi.org/10.1007/978-3-319-46904-1>
- Bjarkam, C. R., Glud, A. N., Orlowski, D., Sørensen, J. C. H., & Palomero-Gallagher, N. (2017). The telencephalon of the Göttingen minipig, cytoarchitecture and cortical surface anatomy. *Brain Structure & Function*, 222(5), 2093–2114. <https://doi.org/10.1007/s00429-016-1327-5>
- Bley, T. A., Wieben, O., François, C. J., Brittain, J. H., & Reeder, S. B. (2010). Fat and water magnetic resonance imaging: Fat and water MRI. *Journal of Magnetic Resonance Imaging*, 31(1), 4–18. <https://doi.org/10.1002/jmri.21895>
- Bode, G., Clausing, P., Gervais, F., Loegsted, J., Luft, J., Nogues, V., & Sims, J., under the auspices of the Steering Group of the RETHINK Project (2010). The utility of the minipig as an animal model in regulatory toxicology. *Journal of Pharmacological and Toxicological Methods*, 62(3), 196–220. <https://doi.org/10.1016/j.vascn.2010.05.009>
- Chung, B. S., Chung, M. S., Lee, S.-B., Youn, C., & Park, J. S. (2018). Sectioned images of a cat head to contribute to learning of its sectional anatomy. *International Journal of Morphology*, 36(2), 537–543. <https://doi.org/10.4067/S0717-95022018000200537>
- Corte, G. M., Hünigen, H., Richardson, K. C., Niehues, S. M., & Plendl, J. (2019). Cephalometric studies of the mandible, its masticatory muscles and vasculature of growing Göttingen Minipigs—A comparative anatomical study to refine experimental mandibular surgery. *PLoS One*, 14(4), e0215875. <https://doi.org/10.1371/journal.pone.0215875>
- Corte, G. M., Plendl, J., Hünigen, H., Richardson, K. C., Gemeinhardt, O., & Niehues, S. M. (2017). Refining experimental dental implant testing in the Göttingen Minipig using 3D computed tomography—A morphometric study of the mandibular canal. *PLoS One*, 12(9), e0184889. <https://doi.org/10.1371/journal.pone.0184889>
- Czeibert, K., Baksa, G., Grimm, A., Nagy, S. A., Kubinyi, E., & Petneházy, Ö. (2019). MRI, CT and high resolution macro-anatomical images with cryosectioning of a Beagle brain: Creating the base of a multimodal imaging atlas. *PLoS One*, 14(3), e0213458. <https://doi.org/10.1371/journal.pone.0213458>
- Del Grande, F., Santini, F., Herzka, D. A., Aro, M. R., Dean, C. W., Gold, G. E., & Carrino, J. A. (2014). Fat-suppression techniques for 3-T MR imaging of the musculoskeletal system. *Radiographics*, 34(1), 217–233. <https://doi.org/10.1148/rg.341135130>
- Delfaut, E. M., Beltran, J., Johnson, G., Rousseau, J., Marchandise, X., & Cotten, A. (1999). Fat suppression in MR imaging: Techniques and pitfalls. *Radiographics*, 19(2), 373–382. <https://doi.org/10.1148/radiographics.19.2.g99mr03373>
- Dondelinger, R. F., Ghysels, M. P., Brisbois, D., Donkers, E., Snaps, F. R., Saunders, J., & Devière, J. (1998). Relevant radiological anatomy of the pig as a training model in interventional radiology. *European Radiology*, 8(7), 1254–1273. <https://doi.org/10.1007/s003300050545>
- Epstein, S. E., Luger, D., & Lipinski, M. J. (2017). Large animal model efficacy testing is needed prior to launch of a stem cell clinical trial: An evidence-lacking conclusion based on conjecture. *Circulation Research*, 121(5), 496–498. <https://doi.org/10.1161/CIRCRESAHA.117.311562>
- Ettrup, K. S., Sørensen, J. C., & Bjarkam, C. R. (2010). The anatomy of the Göttingen minipig hypothalamus. *Journal of Chemical Neuroanatomy*, 39(3), 151–165. <https://doi.org/10.1016/j.jchemneu.2009.12.004>
- Kararli, T. T. (1995). Comparison of the gastrointestinal anatomy, physiology, and biochemistry of humans and commonly used laboratory animals. *Biopharmaceutics & Drug Disposition*, 16(5), 351–380. <https://doi.org/10.1002/bdd.2510160502>
- Kyllar, M., Stembírek, J., Putnová, I., Stehlík, L., Odehnalová, S., & Buchtová, M. (2014). Radiography, computed tomography and magnetic resonance imaging of craniofacial structures in pig. *Anatomia, Histologia, Embryologia*, 43(6), 435–452. <https://doi.org/10.1111/ah.12095>
- Nickel, R., Schummer, A., & Seiferle, E. (2003a). *Lehrbuch der Anatomie der Haustiere, Band I: Bewegungsapparat (8., unveränderte Auflage)*. Stuttgart: Enke.
- Nickel, R., Schummer, A., & Seiferle, E. (2003b). *Lehrbuch der Anatomie der Haustiere, Band IV: Nervensystem, Sinnesorgane, Endokrine Drüsen (4., unveränderte Auflage)*. Stuttgart: Enke.
- Nickel, R., Schummer, A., & Seiferle, E. (2004a). *Lehrbuch der Anatomie der Haustiere, Band II: Eingeweide (9. unveränderte Auflage)*. Stuttgart: Enke.
- Nickel, R., Schummer, A., & Seiferle, E. (2004b). *Lehrbuch der Anatomie der Haustiere, Band III: Kreislaufsystem, Haut und Hautorgane (4., unveränderte Auflage)*. Stuttgart: Enke.
- Noda, Y., Goshima, S., Kozaka, K., Yoneda, N., Mizuno, N., Kato, A., Fujimoto, K., Tsuji, Y., Miyoshi, T., Kawada, H., Kawai, N., Tanahashi, Y., & Matsuo, M. (2018). Optimal window settings in single-source dual-energy computed tomography of the abdomen. *European Journal of Radiology*, 109, 204–209. <https://doi.org/10.1016/j.ejrad.2018.10.012>
- Park, H. S., Shin, D. S., Cho, D. H., Jung, Y. W., & Park, J. S. (2014). Improved sectioned images and surface models of the whole dog body. *Annals of Anatomy = Anatomischer Anzeiger*, 196(5), 352–359. <https://doi.org/10.1016/j.aanat.2014.05.036>
- Popesko, P. (1978). *Atlas of topographical anatomy of the domestic animals (2 edn)*. : W B Saunders Co.
- Rivero, M. A., Ramírez, J. A., Vázquez, J. M., Gil, F., Ramírez, G., & Arencibia, A. (2005). Normal Anatomical Imaging of the Thorax

- in Three Dogs: Computed Tomography and Macroscopic Cross Sections with Vascular Injection. *Anatomia, Histologia, Embryologia*, 34(4), 215–219. <https://doi.org/10.1111/j.1439-0264.2005.00596.x>
- Saka, B., Wree, A., Anders, L., & Gundlach, K. K. H. (2002). Experimental and comparative study of the blood supply to the mandibular cortex in Göttingen minipigs and in man. *Journal of Cranio-Maxillo-Facial Surgery*, 30(4), 219–225. <https://doi.org/10.1054/jcms.2002.0305>
- Sauleau, P., Lapouble, E., Val-Laillet, D., & Malbert, C.-H. (2009). The pig model in brain imaging and neurosurgery. *Animal*, 3(8), 1138–1151. <https://doi.org/10.1017/S1751731109004649>
- Schachtschneider, K. M., Liu, Y., Mäkeläinen, S., Madsen, O., Rund, L. A., Groenen, M. A. M., & Schook, L. B. (2017). Oncopig soft-tissue sarcomas recapitulate key transcriptional features of human sarcomas. *Scientific Reports*, 7(1), 1–12. <https://doi.org/10.1038/s41598-017-02912-9>
- Seeram, E. (2013). *Computed Tomography - E-Book: Physical Principles, Clinical Applications, and Quality Control* (3 edn). : Saunders.
- Simon, G. A., & Maibach, H. I. (2000). The pig as an experimental animal model of percutaneous permeation in man: Qualitative and quantitative observations—an overview. *Skin Pharmacology and Applied Skin Physiology*, 13(5), 229–234. <https://doi.org/10.1159/000029928>
- Spitzer, V., Ackerman, M. J., Scherzinger, A. L., & Whitlock, D. (1996). The visible human male: A technical report. *Journal of the American Medical Informatics Association: JAMIA*, 3(2), 118–130. <https://doi.org/10.1136/jamia.1996.96236280>
- Swindle, M. M. (1984). Swine as replacements for dogs in the surgical teaching and research laboratory. *Laboratory Animal Science*, 34(4), 383–385.
- Vodička, P., Smetana, K., Dvořánková, B., Emerick, T., Xu, Y. Z., Ourednik, J., Ourednik, V., & Motlík, J. (2005). The miniature pig as an animal model in biomedical research. *Annals of the New York Academy of Sciences*, 1049, 161–171. <https://doi.org/10.1196/annals.1334.015>
- Watanabe, H., Andersen, F., Simonsen, C. Z., Evans, S. M., Gjedde, A., & Cumming, P., & DaNeX Study Group (2001). MR-based statistical atlas of the Göttingen minipig brain. *NeuroImage*, 14(5), 1089–1096. <https://doi.org/10.1006/nimg.2001.0910>
- Westbrook, C., & Talbot, J. (2018). *MRI in Practice*. John Wiley & Sons.
- Xue, Z., Antani, S., Long, L. R., Demner-Fushman, D., & Thoma, G. R. (2012). Window classification of brain CT images in biomedical articles. *AMIA Annual Symposium Proceedings, 2012*, 1023–1029.
- Yun, S. P., Kim, D. H., Ryu, J. M., Park, J. H., Park, S. S., Jeon, J. H., Seo, B. N., Kim, H.-J., Park, J.-G., Cho, K.-O., & Han, H. J. (2011). Magnetic resonance imaging evaluation of Yukatan minipig brains for neurotherapy applications. *Laboratory Animal Research*, 27(4), 309–316. <https://doi.org/10.5625/lar.2011.27.4.309>
- Ziegler, A., Gonzalez, L., & Blikslager, A. (2016). Large animal models: The key to translational discovery in digestive disease research. *Cellular and Molecular Gastroenterology and Hepatology*, 2(6), 716–724. <https://doi.org/10.1016/j.jcmgh.2016.09.003>

How to cite this article: Petnehazy O, Donko T, Ellis R, et al. Creating a cross sectional, CT and MR atlas of the pannon minipig. *Anat Histol Embryol*. 2021;50:562–571. <https://doi.org/10.1111/ah.12657>